Wattmeter based on tunnel-effect magnetoresistance sensor (DOI: 10.1063/5.0205541)

S. Soriano[a] (sandra.soriano@uv.es)

D. Ramírez[a] (corresponding author, e-mail: ramirez@uv.es, phone: #34963544035, fax: #34963544353).

R. García-Gil[a] (garciagi@uv.es)

S. Cardoso[b] (scardoso@inesc-mn.pt)

P. P. Freitas[b] (pfreitas@inesc-mn.pt)

[a]Department of Electronic Engineering, University of Valencia, Avda. de la Universitat, s/n, 46100-Burjassot, Spain.

[b]INESC Microsystems and Nanotechnologies (INESC-MN) and Instituto Superior Tecnico, Universidade de Lisboa, R. Alves Redol 9, Lisbon 1000-029, Portugal.

Abstract

The work shows how the tunnel-effect based magnetoresistance (TMR) technology can be used as a competitive sensing method in electrical current and power processors. The sensor is arranged in a Wheatstone bridge topology and each magnetoresistance was composed by a series connection of 360 magnetic tunnel junction (MTJ) elements with the structure (thickness in nm): 100 SiO_2/5 Ta/15 Ru/5 Ta/15 Ru/5 Ta/5 Ru/20 IrMn/2 $CoFe_{30}$/0.85 Ru/2.6 $CoFe_{40}B_{20}$/1.2 MgO/ 2 $CoFe_{40}B_{20}$/0.21 Ta/4 NiFe/0.20 Ru/6 IrMn/2 Ru/5 Ta/10 Ru. First, the electrical and thermal characteristics of the sensor were evaluated by analyzing its response to DC current sweeps at various temperatures, controlled by a climatic chamber. Nominal values of current sensitivity *S* (0.324 mV/A), bridge output offset voltage $V_{o,s,o}$ (-37.1 mV), bridge input resistance $R_{inp,bridge}$ (0.958 kΩ) and their thermal behavior were obtained (0.0036 mV/A ºC, 0.079 mV/ºC, -0.31 Ω/ºC). Second, an instrumentation system is introduced to characterize the sensor, measuring its sensitivity to AC line currents from the mains up to 10 A_{rms}. Finally, an electronic wattmeter was developed showing the relevant quantities of its design. The circuit ables to interface a TMR Wheatstone bridge to an analogue processor. Power and current measurements were obtained from a 150 V_{rms} AC mains 1.5 kW load with resistive and capacitive components, achieving less than 1% deviation over the expected values. The circuit shown can be used to interface to more complex smart digital engines with active or reactive energy processing capabilities but providing inherent high voltage isolation thanks to its TMR measurement technology.

Keywords: tunnel magnetoresistance, current sensor, electrical power, electronic interface, smart metering.

I. INTRODUCTION

Renewable energy sources such as solar and wind power come with electrical complexities, including bidirectional energy flow, production intermittency, and electrical noise generated by switched energy converters, among other challenges. All of them directly affect the stability of the electrical distribution network and the quality of the service received by the end user. Therefore, it is essential to monitor the state of the network as comprehensively and robustly as possible. This is why the development and deployment of smart electronic meters offer electricity companies and their customers the possibility to know the electrical health of their network at the end point of energy consumption. Among the variables to be monitored, electrical current and power are part of the first group. In Ref [1] the advantages and limitations of current sensing technologies based on shunt resistance, current transformer and Hall sensor applied to smart metering are presented. Ref [2] describes the importance of DC metering and the role that current sensing plays in the legal requirements for accuracy and standardization based on the shunt resistor, open and close loop Hall sensor and fluxgate techniques. In Ref [3] a new diagnostic technology for the last generation of smart electrical meters is presented considering the measurement techniques of shunt, current transformer, Rogowsky coil and Hall effect current sensors.

Recent works describe the use of magnetoresistance (MR) effect based current sensors in the field of smart grid. In Ref [4], the electrical characterization (both DC and AC responses) of a MR Wheatstone bridge sensor is detailed, proposing its application across different points in the infrastructure of a smart grid. However, it does not provide specific electronic designs for smart metering purposes. In Ref [5], a device is developed to measure power in residential lines based on MR sensors although its design and dimensions make it difficult to be applied in end-user electrical metering.

MR current sensing technology is being used to implement electrical current sensors for a wide range of scientific or industrial applications. Some interesting fields where this sensing technology is applied are among other, materials inspection Ref [6-7], industry Ref [8-12], medical monitoring Ref [13] or to monitor the lifetime of electronic components Ref [14]. In all these situations, industry manufacturers provide MR Wheatstone bridges to implement current sensors. However, it is not incorporated as a regular option in the field of electrical energy metering. The advantages of MR technology such as miniaturization, no ohmic self-heating, inherent galvanic isolation and optimal frequency response would produce more robust, secure and compact energy meters.

The present work proposes an electronic circuit to interface a Wheatstone bridge tunnel effect-based MR sensor to continuously monitor electrical current and power. The electronic system has been tested in a single-phase 150 V_{rms} AC mains measuring the power delivered to a 1.5 kW load. The output signals provided by the interface can be easily acquired by digital processors in an energy metering system.

II. SENSOR CHARACTERIZATION

The sensor micro-fabrication was carried out at the INESC-MN facilities Ref [15] and internally configured as a bridge arrangement. Each magnetoresistance was composed by a series connection of 360 magnetic tunnel junctions (MTJ) elements with the structure (thickness in nm): 100 SiO_2/5 Ta/15 Ru/5 Ta/15 Ru/5 Ta/5 Ru/20 IrMn/2 $CoFe_{30}$/0.85 Ru/2.6 $CoFe_{40}B_{20}$/1.2 MgO/ 2 $CoFe_{40}B_{20}$/0.21 Ta/4 NiFe/0.20 Ru/6 IrMn/2 Ru/5 Ta/10 Ru. The stack had a resistance area product of 22.6 k$\Omega\mu m^2$ and was implemented with an area of 2 x 30 μm^2, this structure is represented in Fig. 1. The MTJ elements were defined by optical lithography followed by a self-aligned ion milling and passivation process, the thickness of the substrate was of Si 650 μm. Top contacts were done by lift-off of 300 nm thick of AlSiCu and 15 nm of TiW(N_2) thick films. Each magnetoresistance of the bridge had a 2 x 40 μm^2 dimension and were deposited in a 5.5 x 7.6 mm^2 die.

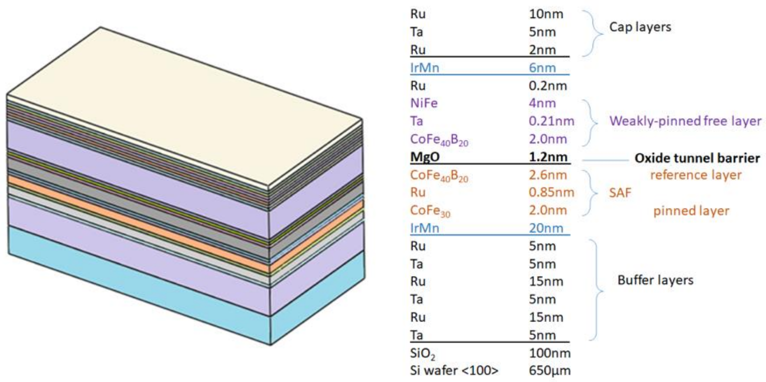

Fig. 1.- Multilayer structure of a MTJ element (CAP: capping layer, SAF: synthetic antiferromagnetic structure).

The sensor was arranged on top of a printed circuit board (pcb) and at the bottom of this, a U-shaped copper track was placed. For electrical and thermal characterization, the sensor was placed inside a climatic chamber, where different temperatures were considered. For each temperature, DC current sweeps were conducted through the copper track. As a result, the sensitivity (S), offset voltage ($V_{off,sensor}$) and input resistance ($R_{inp,bridge}$) of the bridge as well as their thermal behavior were obtained. Fig. 2 shows the DC transfer characteristic of the bridge (sensitivity S) for a current sweep between -10 A and +10 A.

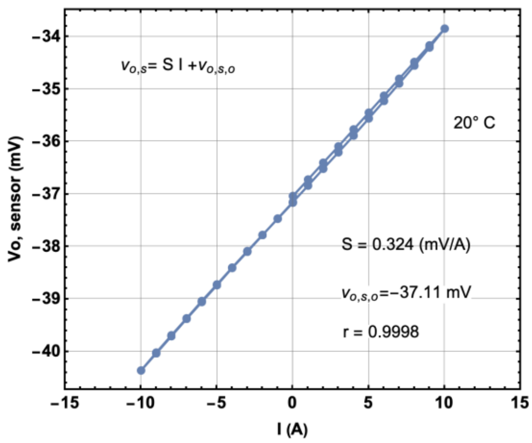

Fig. 2.- Bridge output voltage ($V_{o,sensor}$) dependence with the current I for a sweep between -10 A and +10 A.

Figures 3 a, b and c show respectively the thermal characterization of S, $v_{off,sensor}$ and $R_{inp,bridge}$. Notice that the thermal drift of S and $R_{inp,bridge}$ exhibits opposite signs. With the values recorded in Fig. 3c, it was decided in the next section to bias the bridge with a constant current level of 1 mA, ensuring a sufficient amplitude level at the output of the sensor.

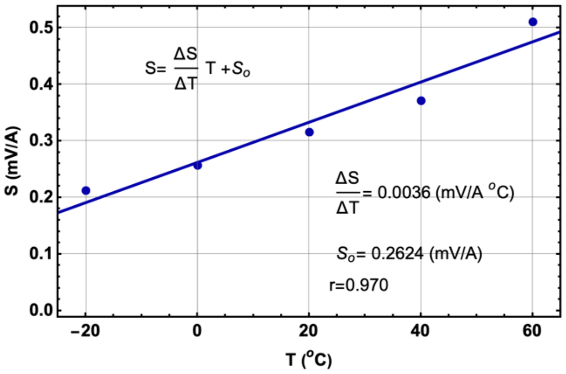

a)

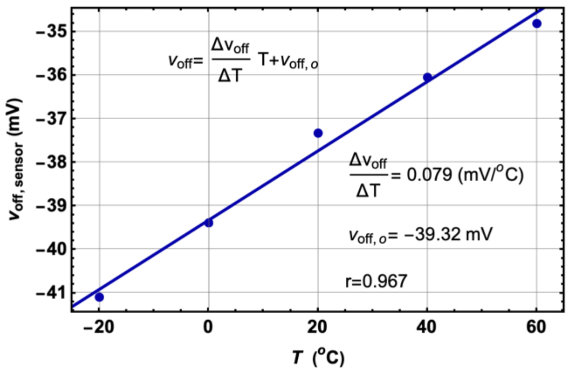

b)

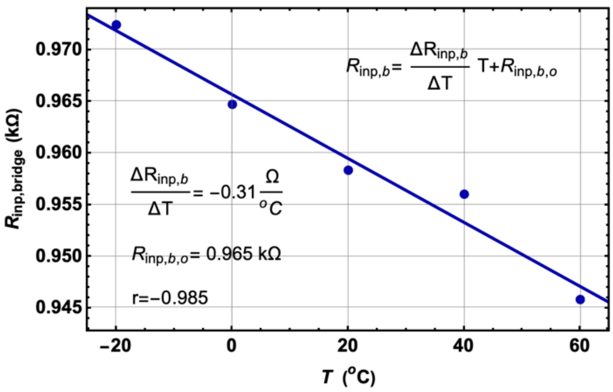

c)

Fig. 3.- Thermal drifts of: a) sensitivity (S), b) offset voltage ($V_{off,sensor}$) and c) input resistance ($R_{inp,bridge}$) of the sensor bridge.

The sensor was applied to measure current and power supplied by a single-phase AC line, so the most important characteristic to consider was its sensitivity to 50 Hz AC line currents. For this purpose, a specific set-up was designed (shown in Fig. 4) where a voltage-controlled AC current calibrator (PCS2B) supplied a current up to 10 A_{rms} controlled by a waveform function generator (HP33521A). The sensor response was measured by the differential preamplifier (ADA400A) and finally acquired by the oscilloscope (DS1074Z). Fig. 5 shows an experimental AC current sensitivity S_S of 0.289 mV/A. This sensitivity value enables the adjustment of the gain of an instrumentation amplifier to suitable values.

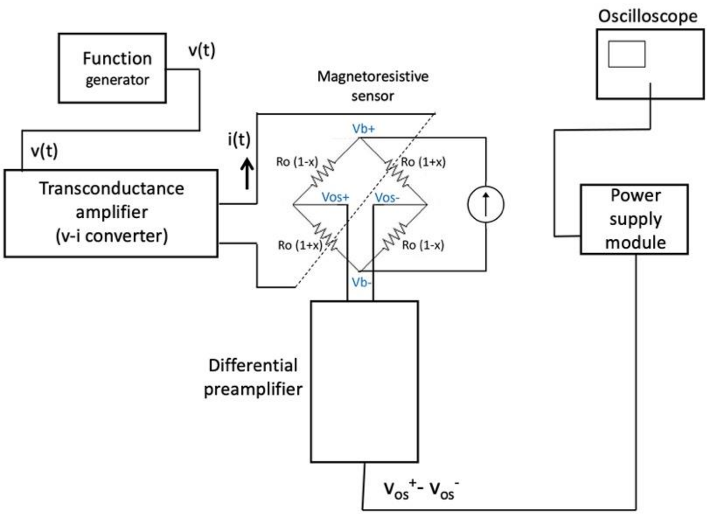

Fig. 4.- Experimental set-up developed to obtain the sensor sensitivity to AC line currents.

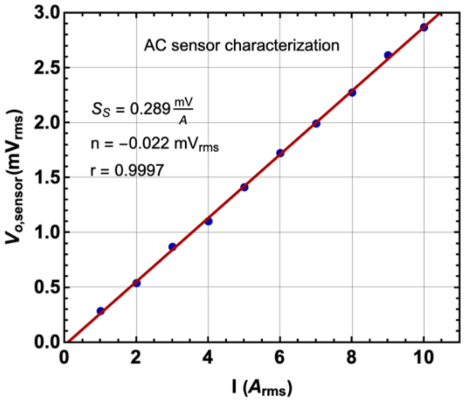

Fig. 5.- RMS output voltage response of the sensor bridge to 50 Hz AC currents.

III. DESIGN OF THE WATTMETER BASED ON TMR SENSOR

The designed wattmeter was based on a TMR Wheatstone bridge current sensor connected to an electronic interface that outputs two electrical voltages related to power and current in the load (Figure 6). It distinguishes the AC-line current $i_{ac}(t)$ and voltage $v_{ac}(t)$ conditioning subsystems and the power and current processing subsystems. The current through the load $i_{ac}(t)$ is measured by biasing the bridge *(R1-R2-R3-R4)* with a constant current level of 1 mA (R_z-Z_1-*R-OA1*), high-pass filtering its output (R_a-R_b-*C*) and conditioning the resulting signal by an instrumentation amplifier (IA) of adequate gain (R_g-*INA118*). An offset *(OA2-REF02)* is added to this output in order to accommodate this signal to the input of the power processor. The measurement of the load voltage is carried out using a voltage transformer decreasing the AC voltage levels. The resistive network placed on its secondary side provides a DC level to adapt the secondary voltage to values appropriate for the V^+ and V^- inputs of the processor. Power and current signals referred to the load are provided by the processor LT2940 which basically is a four-quadrant multiplier that allows the measurement of energy flow in the forward and reverse directions Ref [16]. Voltage signals in its I_{mon} and P_{mon} pins, i. e. $v_{I_{mon}}(t)$ and $v_{P_{mon}}(t)$ are directly related to current and power in the load. The design of the current and power measurement channels is shown below.

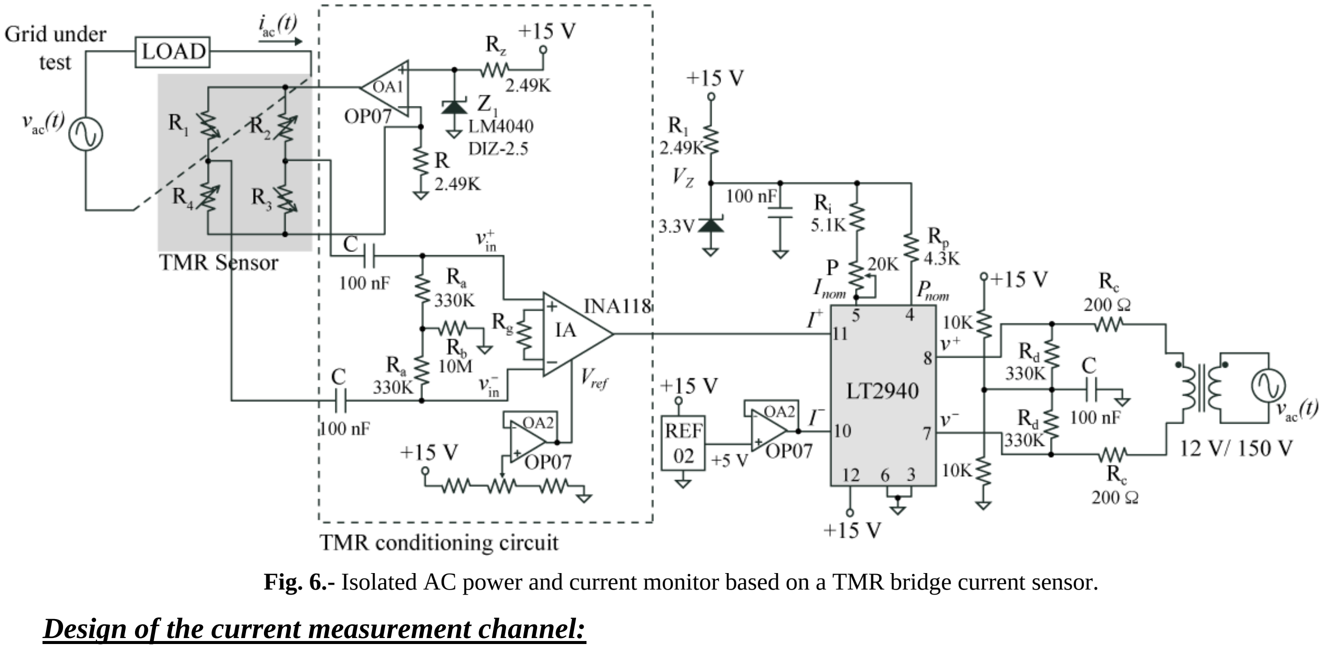

Fig. 6.- Isolated AC power and current monitor based on a TMR bridge current sensor.

Design of the current measurement channel:

The I_{mon} terminal (pin 5 of the LT1940 processor) instantly monitors the current flowing through the load by its voltage $v_{I_{mon}}(t)$. According to Figure 6:

$$v_{I_{mon}}(t) = V_Z + i_{I,mon}(t) \times R_{i,mon} = V_Z + G_{i,mon} \times [v_{I^+}(t) - v_{I^-}(t)] \times R_{i,mon} \quad (1)$$

with $R_{i,mon} = R_i + P$, $G_{i,mon}$ the conversion factor of the current channel, Ref [16] and $[v_{I^+}(t) - v_{I^-}(t)]$ the voltage difference at pins I^+ and I^- respectively.

The voltage at terminal I^+ is the output of the IA, that is:

$$v_{I^+}(t) = G_{INA} \times [v_{in}^{+}(t) - v_{in}^{-}(t)] + V_{ref} \quad (2)$$

The difference $v_{in}^{+}(t) - v_{in}^{-}(t)$ is the sensor output voltage once high-pass filtered by the network (R_a-R_b-C) which eliminates the possible offset that the bridge may have and is expressed by:

$$v_{in}^{+}(t) - v_{in}^{-}(t) = S_s \times i_{ac}(t) \quad (3)$$

where S_S is the nominal sensitivity of the sensor (slope in the characteristic of Figure 5) and $i_{ac}(t)$ the current to be measured.

Voltages on the I^+ and I^- terminals must be equal or greater than 4 V with respect to ground. This condition is achieved at terminal I^- through the voltage reference REF02 (5 V) and at the I^+ terminal through an adjustable voltage at the Ref pin of the IA. In this way it is possible to adequately compensate for the possible offset existing in the current channel of the processor.

If the peak amplitudes are considered, the sensitivity of the current channel will be given by:

$$\frac{\Delta V_{I,mon,pk}}{\Delta I_{pk}} = G_{i,mon} \times G_{INA} \times S_S \times R_{i,mon} \quad (4)$$

In the case of the design carried out there is:

$G_{i,mon}$ = 1 mA/V (nominal value of the current channel conversion factor, Ref [16])

V_{ref} = 3.29 V (experimental voltage value of the Zener diode)

G_{INA} = 28.8 (experimentally adjusted gain for R_g = 1.793 kΩ)

$R_{i,mon}$ = 17.7 kΩ (experimental value obtained by R_i+P)

With the combined values of G_{INA} and $R_{i,mon}$ it is achieved that the maximum current to be measured does not exceed the maximum voltage allowed by the I_{mon} pin ($V_{I,mon,pk} \leq 7.5$ V) according to the manufacturer, Ref [16].

S_S = 0.2896 mV_{pk}/A_{pk} (sensor experimental sensitivity obtained in the characterization process, Figure 5).

In this way, the current channel sensitivity was: $\Delta V_{mon,pk}/\Delta I_{pk} = 131.3\ mV_{pk}/A_{pk}$.

<u>Design of the power measurement channel:</u>

The P_{mon} terminal (pin 4 of the LT1940 processor) instantly monitors the power delivered to the load by its voltage $v_{P_{mon}}(t)$. According to Figure 6:

$$v_{P_{mon}}(t) = V_z + i_{P,mon}(t) \times R_P \quad (5)$$

where, considering the design expressions of the processor,

$$i_{P_{mon}}(t) = K_{P,mon} \times [v^+(t) - v^-(t)] \times [v_{I^+}(t) - v_{I^-}(t)] \quad (6)$$

The difference $[v^+(t) - v^-(t)]$ is the voltage on the secondary side of the voltage transformer attenuated by the R_d-R_c-C network (see Figure 6):

$$v^+(t) - v^-(t) = K_v \times n \times v_{ac}(t) \quad (7)$$

with $K_v = \frac{R_d}{R_d + R_c}$ the attenuation factor of the network R_c-R_d, n the transformer turns ratio and $K_{P,mon}$ the power channel conversion factor (500 µA/V^2 nominal value, Ref [16]). Then from (5):

$$v_{P_{mon}}(t) = V_z + R_P \times K_{P,mon} \times K_v \times n \times G_{INA} \times S_S \times p(t) \quad (8)$$

being $p(t) = v_{ac}(t) \times i_{ac}(t)$. Assuming that the line voltage can be expressed by $v_{ac}(t) = V_{pk} \times \sin 2\pi f t$ and the current through the load by $i_{ac}(t) = I_{pk} \times \sin(2\pi f t + \varphi)$ shifted φ radians with respect to the voltage, then the voltage $v_{P,mon}(t)$ will be given by:

$$v_{P_{mon}}(t) = V_{ref} + \frac{1}{2} \times R_P \times K_{P,mon} \times K_v \times n \times G_{INA} \times S_S \times V_{pk} \times I_{pk} \times \cos\varphi - \frac{1}{2} \times R_P \times K_{P,mon} \times K_v \times n \times G_{INA} \times S_S \times V_{pk} \times I_{pk} \times \cos(4\pi f t + \varphi) \quad (9)$$

Equation 9 indicates that $v_{P,mon}(t)$ is composed of a variable DC level depending on the current I_{pk} and the power factor cos φ (type of the load) and by an AC component of frequency 2 f.

The average value of $v_{P,mon}(t)$ will be given by:

$$\overline{v_{P_{mon}}(t)} = V_{ref} + \frac{1}{2} \times R_P \times K_{P,mon} \times K_v \times n \times G_{INA} \times S_S \times V_{pk} \times I_{pk} \times \cos\varphi \quad (10)$$

and the power channel sensitivity will be:

$$\frac{\Delta\overline{v_{Pmon}(t)}}{\Delta P_{avg}} = R_P \times K_{P,mon} \times K_v \times n \times G_{INA} \times S_S \times \cos\varphi \quad (11)$$

In the case of the design carried out:

R_p = 4310 Ω

K_{Pmon} = 500 μA/V^2 (nominal value of the power channel conversion factor, Ref [16])

K_v = 0.254 (experimental value of the line voltage attenuation factor)

n = 0.055 (transformer turns ratio)

Experimental values of gain G_{INA} and sensor sensitivity S_S have been described above in the design of the current channel.

The sensitivity value of the power channel will be: $\Delta\overline{v_{P_{mon}}(t)}/\Delta P_{avg} = 0.252\ mV/W$.

IV. EXPERIMENTAL PROCEDURE AND RESULTS

For the experimental validation of the designed wattmeter, two types of loads connected to the AC mains were considered: resistive loads (such as electric heaters and rheostats) and capacitive loads (such as a bank of capacitors). Figure 7 shows a schematic of the load used to switch between both configurations. Experimental results were collected using numerical graphs that display the power and current behavior, their relative uncertainties, and with experimental oscilloscope waveforms.

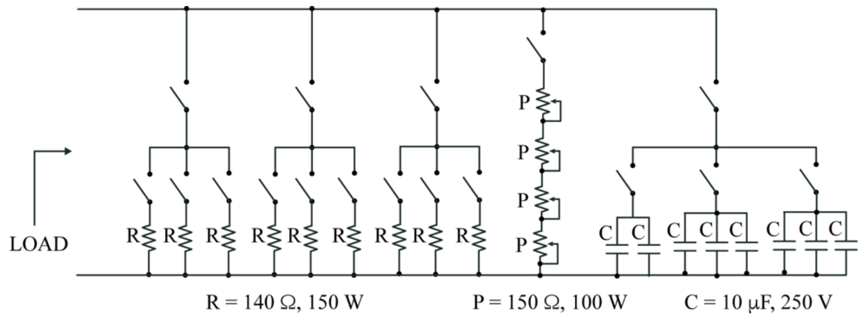

Fig. 7.- Resistive/capacitive load used to monitor its power and current from a 150 V_{rms} AC mains.

Figure 8 shows the experimental rms voltage of the current channel I_{mon} for a current sweep up to 10 A_{rms}. The sweep was generated by the PCS-2B current calibrator (Figure 4), confirming a high degree of linearity and in good agreement with the current channel sensitivity obtained in the previous section.

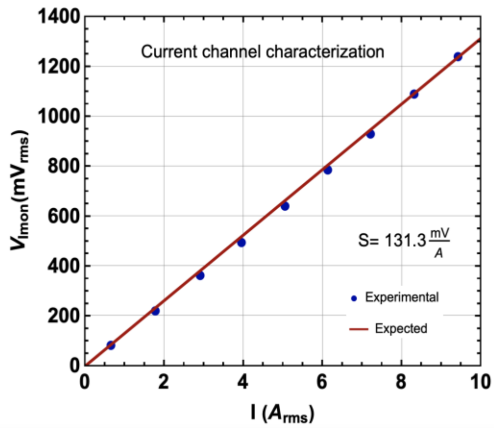

Fig. 8.- Experimental RMS voltage response of the current channel I_{mon}.

To test the accuracy of the power channel P_{mon} a set of different powers were selected switching the resistive and capacitive components of the load (Figure 7). Figures 9 and 10 show the experimental average voltage values of the channel output P_{mon}, first, using a resistive load (Figure 9.a) and then with an 80 μF added capacitance (Figure 10.a). The deviation to the expected values is shown in Figures 9.b) and 10.b) for resistive and resistive and capacitive loads, respectively. As observed a value lower than 1% was achieved in any case.

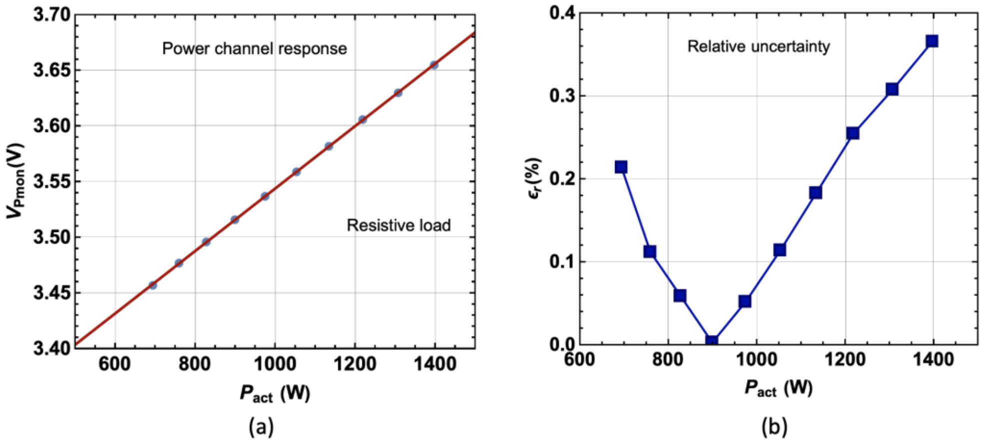

Fig. 9.- Experimental results of (a) voltage power channel V_{Pmon} with resistive load and (b) its relative uncertainty.

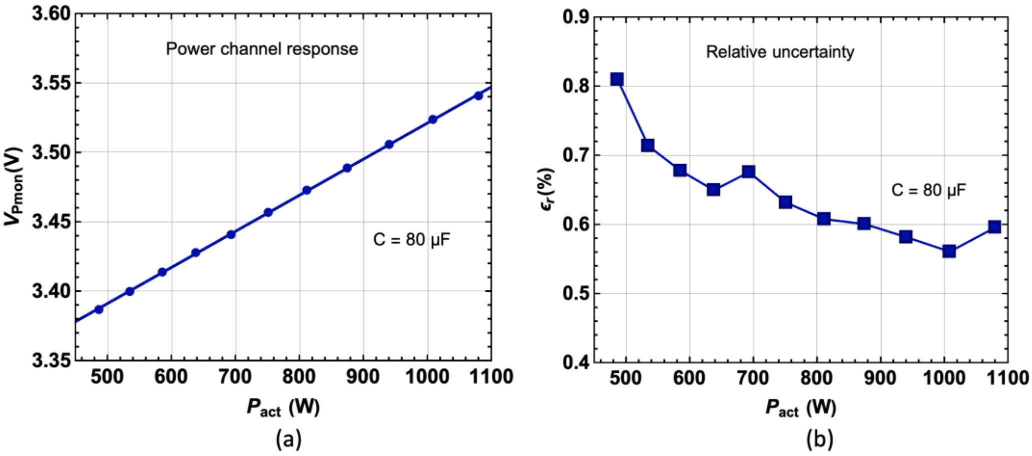

Fig. 10.- Experimental results of (a) voltage power channel V_{Pmon} with resistive and capacitive load (C = 80 μF) and (b) its relative uncertainty.

Figure 11.a) represents the voltage of the current channel, $v_{I_{mon}}(t)$ and the output voltage $v_{I^+}(t) - v_{I^-}(t)$ of the sensor conditioning circuit. Figure 11.b) shows the voltages of the power channel, $v_{P_{mon}}(t)$ and the current channel $v_{I^+}(t) - v_{I^-}(t)$, with the secondary AC mains voltage, $v_{2^o}(t)$, all traces at maximum load (resistive) of 1403 W.

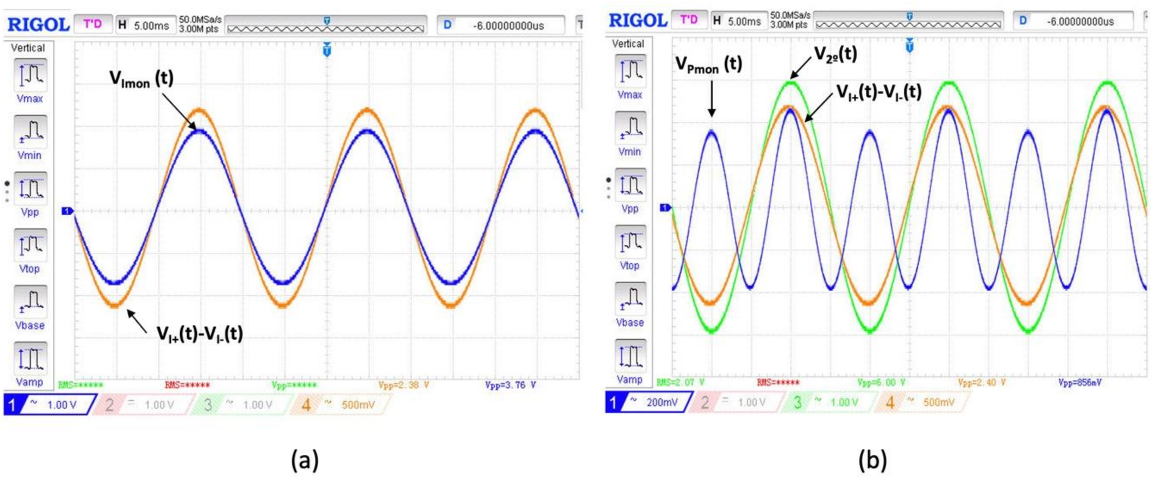

Fig. 11.- (a) blue trace: current channel voltage, $v_{I_{mon}}(t)$, orange trace: output of the conditioning circuit from the sensor, $v_{I^+}(t) - v_{I^-}(t)$, (b) blue trace: power channel voltage, $v_{P_{mon}}(t)$, green trace: secondary AC mains voltage, $v_{2^o}(t)$ and orange trace: output of the conditioning circuit from the sensor, $v_{I^+}(t) - v_{I^-}(t)$ all at maximum load (resistive) of 1403 W.

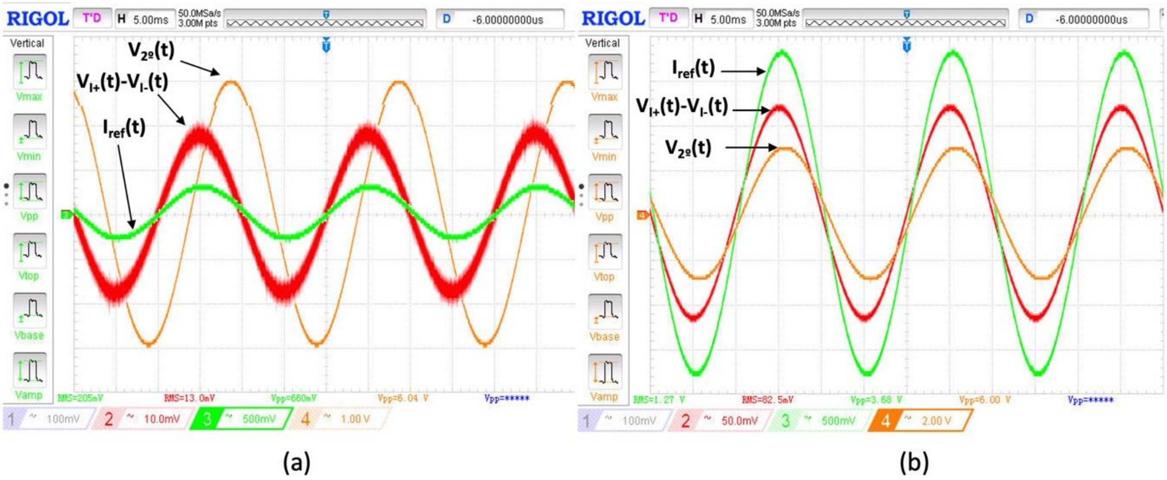

Fig. 12.- (a) cos φ = 0.434, 97.4 W, (b) cos φ = 0.990, 1400 W, orange trace: secondary AC mains voltage, $v_{2º}(t)$), green trace: load current $I_{ref}(t)$ from an AC current probe (TCP202, Tektronix) and read trace: output of the conditioning circuit from the sensor, $v_{I^+}(t) - v_{I^-}(t)$.

Figure 12.a) and b) show the existing phase shift between conditioned load current $v_{I^+}(t) - v_{I^-}(t)$ and secondary AC line voltage $v_{2º}(t)$, corresponding to a cos φ power factor of 0.434 and 0.990 respectively. $I_{ref}(t)$ was the current measured by a reference current probe (TCP202A, Tektronix). Figure 13 shows a physical implementation of the wattmeter made on a printed circuit board.

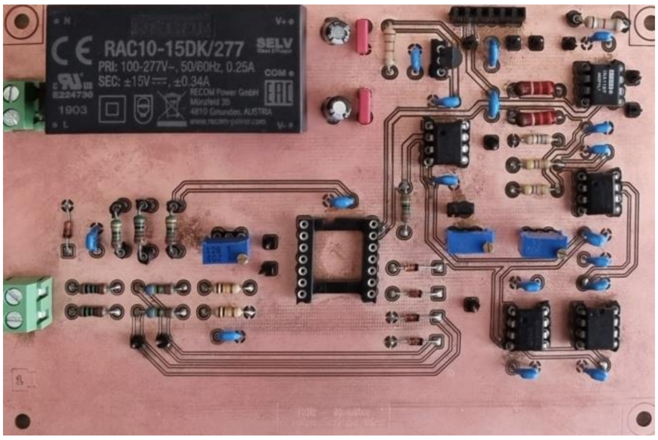

Fig. 13.- Wattmeter prototype in a printed circuit board.

V. CONCLUSIONS

In this work, an electronic circuit that interfaces a Wheatstone bridge current sensor with an analog power processor has been designed and analyzed. Power and current measurements were measured from a 1.5 kW load connected to a 150 V_{rms} AC mains. The accuracy obtained was less than an 1% of deviation over the expected values for resistive load and with a capacitive component. The electronic circuit shown can be used to interface these signals to more complex smart digital engines with active or reactive energy processing capabilities, while providing inherent high voltage isolation thanks to its TMR current measurement technology. Considering the nature of the load, the circuit can be applied to monitor real-time power and current in any combination of load such as resistive, reactive, or non-linear devices like switched mode power converters. TMR technology offers a competitive sensing technique in power control loops, circuit breakers or energy meters where other technologies like shunts, with self-heating and without isolation, or Hall sensors, with their high volume due to magnetic core presence, are commonly used.

VI. AUTHOR DECLARATIONS

The authors have no conflicts to disclose.

Author contributions

S. Soriano: data curation (supporting), investigation and methodology (supporting), writing/draft preparation (supporting). **D. Ramírez**: Conceptualization (lead), data curation (lead), investigation and methodology (equal), resources (lead), supervision and validation (equal), writing/draft preparation (lead). **R. García-Gil**: Writing/draft preparation (supporting). **S. Cardoso**: investigation (lead), methodology (lead), supervision and validation (equal). **P. P. Freitas**: Investigation (lead), methodology (lead).

VII. REFERENCES

1. O'Driscoll, E., O'Donnell, G. E., Industrial power and energy metering-a state-of-the-art review, *Journal of Cleaner Production* 41 (2013) 53-64.
2. Martini, L., DC Energy Metering Applications, *Analog Dialog*, **2021**, 55, n. 1 February, Available at https://www.analog.com/en/analog-dialogue/articles/dc-energy-metering-applications.html, February, 2024.
3. Carriero C., Advances in Smart Electricity Meter Field Diagnostics, Analog Devices Technical Article, Available at https://www.analog.com/en/technical-articles/advances-in-smart-electricity-meter-field-diagnostics.html, February, 2024.
4. Ouyanga, Y.; Wanga, Z.; Zhaoa, G.; Hua, J.; Jia, S.; Hea, J.; Wangb, S. X., Current sensors based on GMR effect for smart grid applications, *Sensors and Actuators A* **2019**, 294, 8–16, https://doi.org/10.1016/j.sna.2019.05.002.
5. Liu, X., He, W., Guo, P., Yang, Y., Guo, T., Xu, Z., Semi-Contactless Power Measurement Method for Single-Phase Enclosed Two-Wire Residential Entrance Lines, IEEE Transactions on Instrumentation and Measurement, vol. 71, 2022.
6. Jin, Z.; Arif, M.; Oogane, M.; Ando, Y., Serial MTJ-Based TMR Sensors in Bridge Configuration for Detection of Fractured Steel Bar in Magnetic Flux Leakage Testing, *Sensors* **2021**, 21, 668. https://doi.org/10.3390/s21020668
7. Rifai, D.; Abdalla, A. N.; Razali, R., Ali, K.; Faraj, M. A., An Eddy Current Testing Platform System for Pipe Defect Inspection Based on an Optimized Eddy Current Technique Probe Design, *Sensors* **2017**, 17, 579; doi:10.3390/s17030579.
8. Sreevidya P. V.; Borolea, U. P.; Kadama, R.; Khana, J.; Barshiliaa, H. C.; Chowdhurya, P., A novel AMR based angle sensor with reduced harmonic errors for automotive applications, *Sensors and Actuators A* **2021,** 324**,** 112573, https://doi.org/10.1016/j.sna.2021.112573.
9. Ripka, P.; Blažek, J.; Mirzaei, M.; Lipovský, P.; Šmelko, M.; Draganová, K., Inductive Position and Speed Sensors, *Sensors* **2020**, 20, 65; doi:10.3390/s20010065
10. Dabek, M.; Wisniowski, P.; Kalabinskia, P.; Wronac, J.; Moskaltsova, A.; Cardoso, S.; Freitas, P. P., Tunneling magnetoresistance sensors for high fidelity current waveforms monitoring, *Sensors and Actuators A* **2016**, 251 142–147, http://dx.doi.org/10.1016/j.sna.2016.10.001.
11. Hu, X., Duan, X., Zhang, W., Fu, Y., Li, Y., Zhao, P., Deng, X., Yu, C., Wang, J., Design and Optimization of Multi-Stage TMR Sensors for Power Equipment AC/DC Leakage Current Detection, Sensors **2023**, 23(10), 4749; https://doi.org/10.3390/s23104749.
12. Di Paolo, M., TMR Sensors Improve Performance and Reduce Size in Power Applications, Power Electronics News, November 1, **2021**.
13. Beheraa, B.; Borolea, U. P.; Sivajia, A.; Khana, J.; Kumarb, P.; Ananda, C. M.; Barshiliaa, H. C.; Chowdhurya, P.; Jadhavd, J. J., Design and development of GMR based low range pressure sensor for medical ventilator application, *Sensors and Actuators A* **2021**, 321 112581, https://doi.org/10.1016/j.sna.2021.112581.
14. Miao, W., Lam, K. H., Pong, P. W. T., Online Monitoring of Aluminum Electrolytic Capacitors in Photovoltaic Systems by Magnetoresistive Sensors, IEEE Sensors Journal, vol. 20, 2, January 15, **2020**.
15. INESC Microsystems and Nanotechnologies (INESC-MN) and Institute for Nanosciences and Nanotechnologies, R. Alves Redol 9, Lisbon 1000-029, Portugal.
16. LT2940 Power and Current Monitor, Analog Devices, U. S. [Online]. Available at https://www.analog.com/en/products/lt2940.html, February **2024**.